FULL PAPER

Synthesis and Evaluation of the Photocatalytic Activity of Nanostructured Composites Based on SiO$_2$ Recovered by TiO$_2$

Werick Alves Machado[a*]**, Higor de Oliveira Alves**[a]**, Antonio Eduardo da Hora Machado**[a,b]

[a]Universidade Federal de Uberlândia, Instituto de Química, Laboratório de Fotoquímica e Ciência de Materiais. Av. João Naves de Ávila, 2121-Bloco 5K. - CEP38400-900 Uberlândia, Minas Gerais, Brazil. [b]Universidade Federal de Catalão, Unidade Acadêmica Especial de Física, Programa de Pós-Graduação em Ciência Exatas e Tecnológicas. Av. Lamartine P. Avelar, 1120 - CEP 75704-020, Catalão, Goiás, Brazil.

Abstract:

Almost spherical SiO$_2$ nanoparticles were recovered by thin films of TiO$_2$ (highly crystalline anatase) produced in situ sol-gel syntheses. Silica coating was proven by scanning electron microscopy and infrared measurements. The outstanding photocatalytic efficiency of this material was proven by the degradation of the dye Ponceau 4R (P4R) in aqueous solution, by monitoring its discoloration as well as by the photocatalytic production of gaseous hydrogen. In the first case, the color of the solutions submitted to the photocatalytic process was reduced to zero in 140 minutes of reaction. Regarding the hydrogen production, 5.5 mmol of H$_2$ were obtained in 5 hours of reaction, corresponding to a specific rate of production of 13.6 mmol g^{-1}h^{-1}, a value much higher than that obtained using TiO$_2$ P25 (2.66 mmol g^{-1}h^{-1}) under similar conditions, or even with other photocatalysts reported in the literature. This outstanding photocatalytic activity is coherent with the specific surface area and porosity (respectively 70 m^2/g and 15%), estimated for this material. On the other hand, this material presents noticeably superior band gap energy (E$_g$), 3.3 eV, when compared to the typical values found for TiO$_2$. This small discrepancy, of 3%, may be the result of the mixture of electronic states of both materials.

Keywords: titanium dioxide; sol-gel synthesis; TiO2/SiO2 composite; heterogeneous photocatalysis; production of H$_2$

1. Introduction

Titanium dioxide is widely used in environmental photocatalysis [1-3], also showing potential application in the photocatalytic production of hydrogen and in dye solar cells [4-7]. However, the aggregation of TiO$_2$ nanoparticles tends to reduce their specific surface area altering several intrinsic characteristics of the material that end up compromising its application as photocatalyst [8-10].

Its immobilization on the surface of an inert material can be a good strategy to minimize aggregation and related problems, in addition to facilitating the recovery of the catalyst for subsequent reuse. In recent years, the use of photocatalysts immobilized in different materials has shown to be a good strategy to circumvent these difficulties [11-13].

By owning a well-known surface chemistry, optical transparency, thermal and mechanical stability, low cost, easy preparation, high surface area, and to a certain extent, for being photochemically inert [14-16], SiO$_2$ fits perfectly as a support material [17]. In this way, the immobilization of TiO$_2$ on SiO$_2$ surface can lead to a better thermal stability for TiO$_2$ [14]. In addition, this should increase the photocatalytic activity due to the less tendency to aggregation, provided by silica [18], as well as the presence of vacancies of oxygen in the TiO$_2$ supported, which may increase

---

the delay of recombination between the photogenerated pairs [19] and a higher ability of adsorption of reagents [20].

In the present work, nanoparticles of SiO_2 were used as structural support for the purpose of increase the photocatalytic activity of TiO_2. The synthesized material was characterized by different techniques, besides having had its photocatalytic activity evaluated both in terms of degradation of organic matter and production capacity of H_2.

2. Results and Discussion

2.1 Characterizations

After synthesis and posterior treatments, the TiO_2/SiO_2 composite was characterized by x-ray diffraction in order to check your structure and crystalline phase (**Figure 1**). Based on the JCPDS (21-1272) crystallographic record it was verified the existence of only a highly crystalline anatase phase. It is very probable that this is due to the heat treatment performed in combination with the presence of silica, which guarantees a higher thermal stability to the anatase phase [14].

The peaks related to anatase correspond to the values of 2θ equal to 25.4º, 37.8°, 38.4°, 48.0°, 54.1°, 55.2°, 62.5°, 69.0°, 70.2°, 75.3° and 82.7°, identified in the diffratogram, **Figure 1**, which correspond respectively to the planes (101), (004), (112), (200), (105), (211), (204), (116), (220), (215) and (224). The peaks identified at 44.5°, 64.9° e 78.3° are related to the constituent material of the sample holder (aluminum), according to JCPDS crystallographic record (1-1180). The absence of peaks referring to silica is due the fact that this material is present in amorphous form (**Figure S1**) [21].

By applying the Scherrer equation [22], the average size of the crystallites was estimated as being equal to 10 nm. From what has been reported in the literature, this parameter depends on the type of heat treatment for which the material is submitted. It has been reported to anatase, for example, crystallite sizes of 18 nm and 25 nm, for TiO_2 thermally treated by muffle at 400°C during 5 or 6 hours [23,24]. The main morphological data are presented in **Table 1**. For an anatase synthesized by hydrothermal route (pH > 7 and 200ºC, for 2h), a crystallite size equivalent to that estimated in the present study was reported [25]. This suggests that the presence of silica should have provided the composite with a significant reduction in the size of the crystallite, most likely due the suppression of the processes of growth and surface diffusion of the nanoparticles of TiO_2, partly due the curvature of the SiO_2 surface and formation of interfacial bonds between the oxides [26].
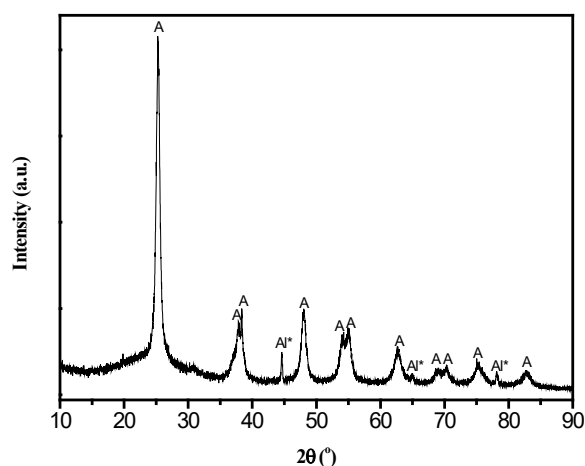

Figure 1. Diffractogram obtained for the TiO_2/SiO_2 composite. The peaks indicated with "A" are attributed to the anatase phase of TiO_2 and "Al*" refers to the sample holder (Aluminum).

From the diffuse reflectance spectra, converted into Kubelka-Munk functions, and applying the direct method [27], **Figure 2**, it was possible to estimate the band gap energy (E_g) of the TiO_2 supported as being equal to 3.3 eV (**Table 1**).

Table 1. Main morphologic and electronic properties of the as synthesized composite and some pure photocatalysts reported in the literature.

Photocatalyst	Crystallite size (nm)	Surface area (m^2g^{-1})	Porosity (%)	Band gap (eV)	Ref
TiO_2/SiO_2	10	70	15	3.3	*
TiO_2-1	18	66	15	3.2	23
TiO_2	25	55	12	3.2	24

*This study

84

Orbital: Electron. J. Chem. 11 (2): 83-90, 2019

For the commercial oxide TiO_2 P25, a mixture of anatase and rutile with about 70% anatase, the band gap energy (E_g) reported in the literature is around 3.2 eV [28,29], an equally reported value for pure anatase [23,24]. The slightly higher E_g estimated for the synthesized composites may be related to a possible mixture of electronic states of both materials, highlighting that the amorphous sílica posesses an E_g higher than 8.0 eV [30].
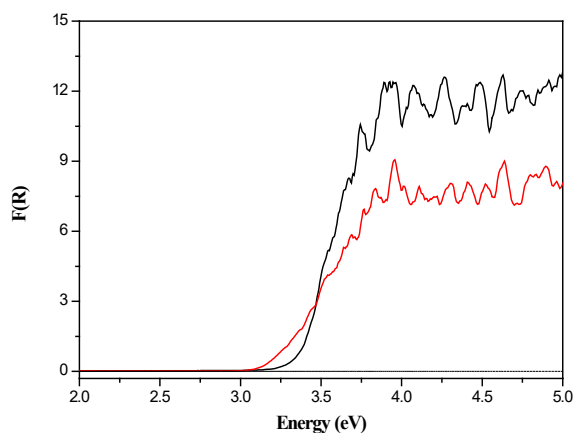

Figure 2. Diffuse reflectance spectra, expressed in terms of Kubelka-Munk function, for the (—) TiO_2/SiO_2 composite and (—)TiO_2 P25.

Figure 3 presents the FT-IR spectra of the pure oxides (SiO_2 and TiO_2) and of the TiO_2/SiO_2 composite.
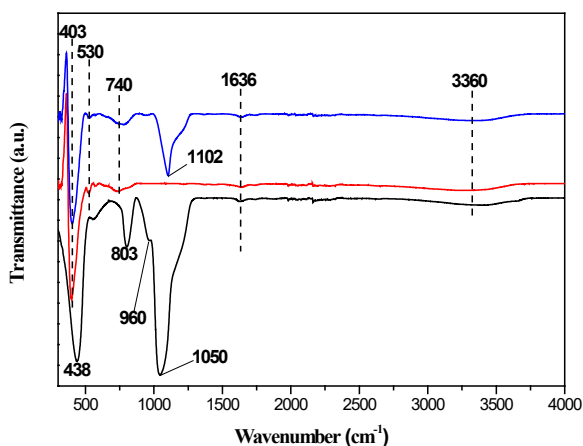

Figure 3. Fourier Transform infrared spectra of (—) SiO_2, (—) TiO_2 and of the composite (—) TiO_2/SiO_2.

As observed, the pure SiO_2 presents three principal vibrations in the IR: a band centered at 438 cm^{-1} related to Si-O-Si bending and the bands at 803 and 1050 cm^{-1}, respectively related to symmetric and asymmetric stretching of Si-O-Si. In addition to these bands, a secondary vibration related to Si-OH is observed at 960 cm^{-1} [31-33]. For the pure TiO_2 three vibration characteristics are observed: a broad and intense band at 403 cm^{-1} and more two subtle band at 530 and 730 cm^{-1}, both related to the Ti-O-Ti stretching [33,34]. Already for the TiO_2/SiO_2 composites, a band centered at 1102 cm^{-1} can be observed in the region attributed to SiO_2 in addition to a band centered at 403 cm^{-1}, related to TiO_2. The SI-O-Si vibration (in general at 1050 cm^{-1}) is slightly shifted to higher frequencies (1102 cm^{-1}) due the calcination of the material at high temperature, suggesting the strengthening of this bond [33]. In all spectra it was possible to observe the occurrence of two relatively wide bands at 1636 cm^{-1} and 3360 cm^{-1} related to the vibration of O-H from H_2O molecules respectively chemisorbed and physisorbed on the surface of the photocatalyst [34,35]. It is important to note that in the IR spectrum of the composites bands were not observed in the range between 1350 to 1560 cm^{-1}, related to the presence of organic residues related to the precursor, attesting the effectiveness of the heat treatment to which the material was submitted after the synthesis [32,36].

In the N_2 adsorption/desorption assays using the BET (Brunauer-Emmett-Teller) method the isotherm obtained (**Figure S2**) is, according to IUPAC, classified as being type IV, characteristic of mesoporous solids with average pore diameter between 2 and 50 nm [7,37]. Besides, the specific surface area was estimated as being 70 m^2/g, with 15% porosity (**Table 1**) and a mean pore diameter of 2.14 nm, calculated using the BJH (Barrett-Joyner-Halenda) method. The oxides synthesized in previous studies [23,24], also using the sol-gel method, presented lower specific surface areas (66 and 55 m^2/g, respectively), suggesting that in the synthesis of TiO_2 the presence of SiO_2 may have favored the reduction of TiO_2 aggregation, increasing its surface area, since it is known that SiO_2 tends to restrict the mobility of TiO_2 crystals [26].

Images obtained by scanning electron microscopy are shown in **Figure 4**. Silica features particles slightly agglomerated with fairly regular spherical shape (**Figure 4a**). For the composites under study it is possible to observe an increase in the particle sizes, indicating the total covering

85

Orbital: Electron. J. Chem. 11 (2): 83-90, 2019

of SiO$_2$ by TiO$_2$ (**Figure 4b**). In addition, it is possible to observe that there was the formation of TiO$_2$ outside the silica surface, possibly due to excess of precursor of titanium used in the synthesis. More images of SiO$_2$ and of the composite in other magnifications are available in the Supplementary Material (**Figures S3** and **S4**).
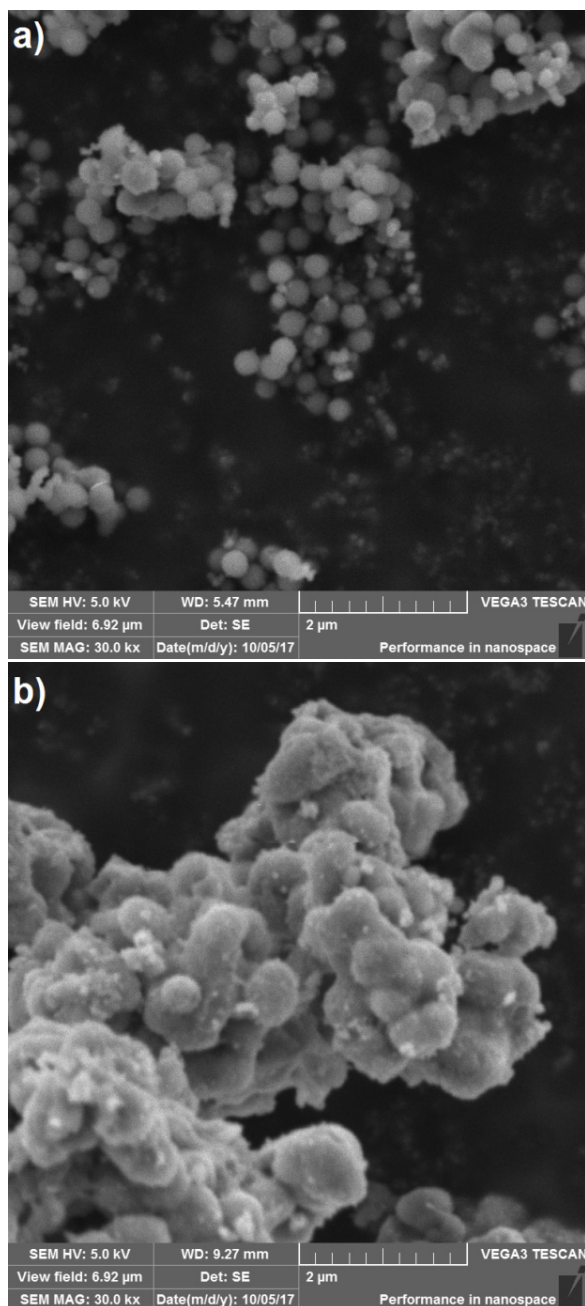

Figure 4. Photomicrographs for (a) SiO$_2$ and for the (b) TiO$_2$/SiO$_2$ composite.

2.2. Photocatalytic activity and hydrogen production

The evaluation of the photocatalytic activity of the synthesized composite was done on a bench scale, both by monitoring the discoloration of aqueous solutions containing the dye Ponceau 4R (P4R) and by the evaluation of the photocatalytic production of hydrogen.

Figure 5 shows the shows the results obtained in photocatalytic tests of dye degradation using the composite TiO$_2$/SiO$_2$, quantified by monitoring the maximum absorbance of the dye at 507 nm. The decrease of P4R concentration follows an exponential decay profile as a function of the irradiation time, **Figure 5 – Insert**.
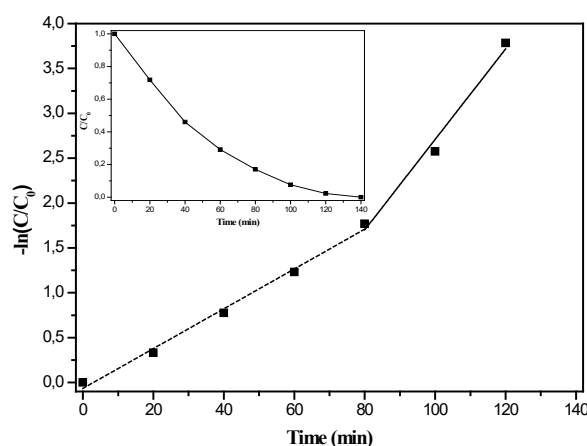

Figure 5. Kinetics of discoloration of the dye Ponceau 4R (P4R) using the composite TiO$_2$/SiO$_2$ as photocatalyst. Insert: Absorbance reduction at 507 nm as a function of reaction time.

The composite presented a good photocatalytic activity, with the elimination of 100% of the color of the dye in 140 minutes of reaction. This is due to the fact that the immobilization of titanium dioxide on the surface of silicon dioxide should have provided a better dispersion of the catalyst, thus avoiding the problems usually related to its aggregation [38,39]. It is well established that the degradation of organic matter, by heterogeneous photocatalysis, follows pseudo-first order kinetics [4, 40, 41]. Based on this premise, the kinetics was adjusted by linear regression of the data of the Neperian logarithm of the concentrations ratio, -ln(C/C$_0$), versus reaction time, **Figure 5**. Based on this figure, the P4R degradation appears to occur in two stages. In the first 80 minutes of reaction the estimated value of the apparent rate constant is 2.2×10^{-2} min^{-1} (R^2=0.9912), increasing

86

Orbital: Electron. J. Chem. 11 (2): 83-90, 2019

to 5.0 x 10^{-2} min^{-1} (R^2= 0.9736) in the last 60 minutes, when the degradation rate practically doubles. This increase in the degradation rate can be explained by the relative growth of the number of reactive species produced by the photocatalyst throughout the process as the concentration of oxidable substrate decreases [42]. Comparatively, the estimated degradation rate of P4R mediated by the composite evaluated in this study is approximately 40% higher than the observed in the degradation of this same substrate in a photocatalytic reaction mediated by TiO$_2$ photocatalysts prepared by the Pechini method [43], and approximately close to that obtained using a TiO$_2$(P25)/ZnPc 1.6% composite, or a TiO$_2$ prepared by the Sol-gel method [43].

Regarding the production of hydrogen, a production of 5.5 mmol of H$_2$ was achieved in 5 hours of reaction. O advance of the reaction is shown in the following figure.
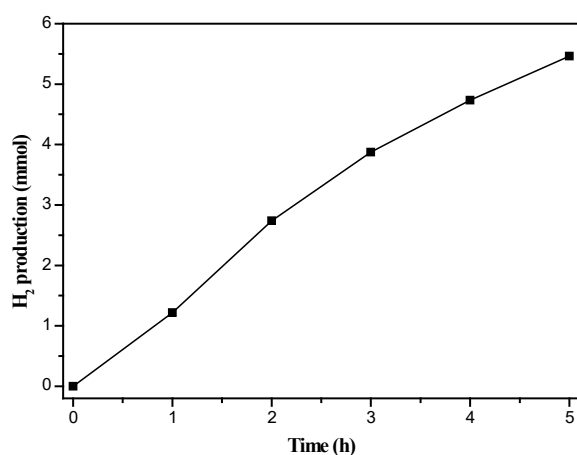

Figure 6. Hydrogen production (mmol) as function of the reaction time using the composite TiO$_2$/SiO$_2$ as photocatalyst, with the addition of a charge of 0.05% m/m of Pt as cocatalyst.

For comparative purposes, in addition to the amount hydrogen produced, the results also can be presented in terms of the specific rate of hydrogen production (SRHP), defined as:

$$SRHP = \frac{n}{t\,m} \qquad \text{Equation 1}$$

In which n is the number of mols of H$_2$ produced, obtained by integration throughout the experiment; t is the total reaction time and m is the mass of photocatalyst (in grams). The SRHP achieved using the composite was of

approximately 13.6 mmol g^{-1}h^{-1}, a result much higher than that obtained using the commercial oxide TiO$_2$ P25 (2.66 mmol g^{-1}h^{-1}) under the same experimental conditions.

In tests using an association between TiO$_2$ (anatase) and ZnO, Xie and coworkers reached a SRHP of 2.15 mmol g^{-1}h^{-1}, but adding to the catalyst 0.5% m/m of Pt [44]. In another study, Zhu synthesized TiO$_2$ (anatase) over carbon nanospheres, carrying this material with Pt 0.1% m/m, achieving an SRHP of 2.85 mmol g^{-1}h^{-1} [45]. It should be noted that in both studies the experimental conditions were similar to those applied in the present study. Considering that these results were the most representative in the mentioned studies, it can be affirmed that the SRHP using the TiO$_2$/SiO$_2$ presented in this work is superior to the reported in these studies. It should be emphasized that the amount of cocatalyst used in this study is much smaller than in the reported studies.

In this way, it is observed that the silica coating by TiO$_2$ obtained by sol-gel synthesis resulted in a promising photocatalyst with excellent performance both in the degradation of P4R as catalytic production of hydrogen gas

3. Material and Methods

Titanium dioxide supported in silicon dioxide was synthesized by the sol-gel method [46]. Prior to its preparation, the SiO$_2$ was synthesized using the Stöber method [47].

3.1. Synthesis of SiO$_2$

15 mL of Milli-Q water and 4 mL of NH$_4$OH (28%, Synth) were added to 100 mL of ethanol (99.8%, Vetec). This mixture was maintained under magnetic stirring for 5 minutes and then 3 mL of tetraethyl orthosilicate (98%, Sigma-Aldrich) were quickly added. From there, the mixture was kept under vigorous stirring for over 1 hour. Finally, the solution was neutralized with 5M HCl solution (P.A., Biotec), centrifuged and dried in an oven at 70 °C for 15 hours.

3.2. Synthesis of the composite TiO$_2$/SiO$_2$

0.2 g of dry silica were dispersed in 80 mL of

87

Orbital: Electron. J. Chem. 11 (2): 83-90, 2019

2-propanol (99.5%, Vetec), being this suspension maintained under magnetic stirring for 5 minutes. Then were added quickly 3 mL of titanium isopropoxide (97%, Sigma-Aldrich), being the mixture maintained under vigorous stirring for 19 hours. Following, using a procedure adapted from Santos et al [24], proceeded to the hydrolysis of the titanium isopropoxide, using a mixture containing 6 mL of 2-propanol and 3 mL of Milli-Q water, which was added slowly to the suspension. This mixture was then kept under magnetic stirring for 1 hour. Finally, the resulting colloidal suspension was centrifuged, and the precipitate was separated and submitted to calcination in muffle at 450 °C for 5 hours. By stoichiometric calculations, the proportion between the two oxides present in the synthesized composite is approximately 80% of TiO_2 and 20% of SiO_2.

3.3. Characterizations

A SHIMADZU XRD-6000 diffractometer coupled with a CuKα (λ= 1.54 nm) monochromatic source were used to evaluate the crystallinity of the composite and its crystalline phase, in the angular range between $10° \leq 2\theta \leq 90°$, with scanning speed of $2°min^{-1}$. The measurements of electronic absorption by diffuse reflectance were performed using a SHIMADZU model 1650-PC spectrophotometer. The infrared spectra were acquired using a Perkin Elmer Frontier Total Attenuated Reflectance FTIR spectrometer. The measurements were done on a diamond crystal plate, using 16 scans with a resolution of 4 cm^{-1}, for each sample. Specific surface area measurements were performed using a Quantachrome model 2000 Surface Area, Pore Size and Distribution Analyzer. For the morphological analysis of the materials, a TESCAN Vega 3 Scanning Electron Microscope was employed.

3.4. Evaluation of the photocatalytic activity and hydrogen production

Photocatalytic assays of P4R degradation were performed using a photocatalytic reactor described in previous studies [43]. A 400 W high-pressure mercury lamp, without the protective bulb, was employed as a source of ultraviolet radiation. Despite its emission spectrum, that covers both the ultraviolet and visible portions of the electronic spectrum [28], only photons with E ≥ 3.2 eV are capable to excite the photocatalyst. The experimental conditions were an aqueous suspension (4L) containing 100 mg L^{-1} of the photocatalyst and 125 mg of the dye (P4R or New Coccine, Dye content 75%, Sigma-Aldrich). The suspension was circulated and irradiated for 140 minutes. The degradation, evaluated in terms of discoloration of the solution, was monitored by spectrophotometric measurements using a SHIMADZU UV – 1201 spectrophotometer.

The hydrogen production assays were carried out employing 75 mg of the photocatalyst loaded with 0.05% m/m of Pt. Platinum, from a solution of chloroplatinic acid hexaidrated in isopropanol, was photochemically reduced at the beginning of the photocatalytic process, by its addition in a mixture containing 600 mL of Milli-Q water and 150 mL of methanol, used as sacrificial reagent (20% v/v). The suspension contained in the reactor was submitted to constant stirring, being irradiated by a high-pressure mercury lamp of 400 W, without the protective bulb.

The reactor, of borosilicate glass, is equipped with a cooling system that involves the part that contains the reaction medium. This cooling system is connected to a thermostated bath adjusted to 15 °C.

The whole process occurred under nitrogen atmosphere.

The quantification of the hydrogen gas produced was performed every 1 hour, employing a Perkin Elmer Clarus 580 gas chromatograph, containing a Porapak-N column and a molecular sieve, coupled to a thermal conductivity detector.

All Photocatalytic assays were performed on a lab scale.

4. Conclusions

TiO_2 nanoparticles were successfully synthesized on the surface of SiO_2 spheres, employing the sol-gel method, giving rise to composites of the type TiO_2/SiO_2. The results obtained, in the level of photocatalytic assays, especially regarding the production of gaseous hydrogen, suggest that the level of coating achieved ensured improved photocatalytic properties to the catalyst.

88

Orbital: Electron. J. Chem. 11 (2): 83-90, 2019

As verified in the characterizations, the presence of silica ensured a higher thermal stability to the anatase, the only phase formed during the synthesis, a reduction in the crystallite size of up to 150% and an increase in the specific surface area of approximately 6% compared to TiO_2 anatase obtained by Santos et al [24]. It was also found that the band-gap energy of the synthesized oxide is slightly higher than that reported for the TiO_2 P25 [28-29] and for the oxides (anatase) synthesized by França et al [23] and Santos et al [24]. By IR and MEV measurements, the coating of the SiO_2 by TiO_2 was confirmed.

The TiO_2/SiO_2 presented a good photocatalytic activity in the degradation of Ponceau 4R, a dye used as a model of oxidative substrate, reaching 100% of degradation in 140 minutes. The degradation achieved, confronted with the results reported by Oliveira et al. [41] under similar experimental conditions, but using TiO_2 synthesized by the Pecchini method, was at least 40% more efficient.

Concerning the hydrogen production assays, the result obtained using the TiO_2/SiO_2 composites was significantly better than that obtained using TiO_2 P25 or even in the comparisons done with similar studies presented in the literature [42-43]. These results indicate that the catalysts presented in this study have high potential for application both in environmental photocatalysis and in the photocatalytic production of hydrogen.

Supporting Information

Figures S1-S4

Acknowledgments

References and Notes

[1] Hashimoto, K.; Irie, H.; Fuijishima, A. *Jpn. J. Appl. Phys.* **2005**, *44*, 8269. [Crossref]

[2] Ahmed S.N.; Haider, H. *Nanotechnology* **2018**, *28*, 342001. [Crossref]

[3] Zhang, T.; Wang, X.; Zhang, X. *Int. J. Photoenergy* **2014**, 607954. [Crossref]

[4] Machado, A. E. H.; Santos, l. M. S.; Borges, K. A.; Batista, P. S.; Paiva, V. A. B.; Muller, P. S.; Oliveira, D. F. M.; França, M. D. Potential applications for solar photocatalysis: from environmental remediation to energy conversion. *Solar Radiation.* Babatunde, E. B., eds. Rijeka: InTech, 2012, chapter 19, 339. [Crossref]

[5] Machado, A. E. H.; Patrocinio, A. O. T.; França, M. D.; Santos, L. D.; Borges, K. A.; Paula, L. F. Metal oxides for photoinduced hydrogen production and dye sensitized solar cell applications. *Materials and processes for energy: communicating current research and technological developments.* : Méndez-Vilas A., ed. Badajoz: Formatex. 2013, 867. [Crossref]

[6] Guayaquil-Sosa, J. F.; Calzada, A.; Serrano, B.; Escobedo, S.; Lasa, H. *Catalysis*, **2017**, *7*, 324. [Crossref]

[7] Machado, A. E. H.; Borges, K. A.; Silva, T. A.; Santos, L. M.; Borges M. F.; Machado, W. A.; Caixeta, B. P.; França, M. D.; Oliveira, S. M.; Trovó, A. G.; Patrocinio, A. O.T. Applications of Mesoporous Ordered Semiconductor Materials — Case Study of TiO_2. *Solar Radiation Applications.* Raphael Bello., eds. IntechOpen, 2015, chapter 5, 87-118. [Crossref]

[8] Kumar, S. G.; Devi, L. G. J. *Phys. Chem. A* **2011,** *115*,1311. [Crossref]

[9] Wang, D.; Li, Y.; Puma, G. L.; Wang, C.; Wang, P.; Zhang, W.; Wang, Q. *J. Hazard. Mater.* **2015**, *285*, 277. [Crossref]

[10] Wang, P.; Qi, N.; Ao, Y.; Hou, J.; Wang, J. Q. *Environ. Pollut.* **2016**, *212*, 178. [Crossref]

[11] Spasiano, D.; Marotta, R.; Malato, S.; Fernandez-Ibañez, P.; Di Somma, I. *Applied Catalysis B: Environmental* **2015**, *170*, 90. [Crossref]

[12] Manasscro, A.; Satuf, M. L.; Alfano, O. M. *Environ. Sci. Pollut. Res.* **2017**, *24*, 6031. [Crossref]

[13] Lopes Cunha, D.; Kuznetsov, A.; Achete, C. A.; Machado, A. E. H.; Marques, M. *Peer J*, **2018**, 1. [Crossref]

[14] Staykov, A.; Neto-Ferreira, E. P.; Cruz, J. M. Y. S.; Ullah, S; Filho-Rodrigues, U. P. *Int. J. Quantum Chem.* **2008,** *118*, 1. [Crossref]

[15] Son, S.; Hwang, S. H.; Kim, C.; Yun, J. Y.; Jang, J. *Nanoscale* **2013**. *3*, 4815. [Crossref]

[16] Zhang, H.; Luo, X.; Xu, J.; Xiang, B.; Yu, D. *J. Phys. Chem. B* **2004**, *108*, 14866. [Crossref]

[17] Dagle, V. L.; Flake, M. D.; Lemmon, T. L.; Lopez, J. S.; Kovarik, L.; Dagle, R. A. *Appl. Catal., B* **2018**, *236*, 576. [Crossref]

[18] Periyat, P.; Baiju, K. V.; Mukundan, P.; Pillai, P. K.; Warrier, K. G. H. *Applied Catalysis A: General*, **2008**, *349*, 13. [Crossref]

[19] Cheng, P.; Zheng, M.; Jin, Y.; Huang, Q. *Mater. Lett.* **2003**, *57*, 2989. [Crossref]

[20] Guo, N.; Liang, Y.; Lan, S.; Liu, L.; Ji, G.; Gan, S.; Zou, H.; Xu. *Appl. Surf. Sci.* **2014**, *305*, 562. [Crossref]

89

Orbital: Electron. J. Chem. 11 (2): 83-90, 2019

[21] Roque-Ruiz, J. H.; Máynez-Martínes, H.; Garibay-Zalapa, a.; Moraquecho-Arizmendi, A.; Farias, R.; López-Reyes, S. Y. *Results Phys.* **2017**, *7*, 2520. [Crossref]

[22] Lessing, P. A.; Tai, L. W.; Anderson, H, U. *Am. Ceram. Soc. Bull.* **1989**, *68*, 1002.

[23] Patrocinio, A. O. T.; Schneider, J.; França, M. D.; Santos, L. M.; Caixeta, B. P.; Machado, A. E. H.; Bahnemann, D. W. *RSC Advances*, **2015**, *5*, 70536. [Crossref]

[24] Santos, L. M.; Machado, W. A.; França, M. D.; Borges, K. A.; Paniago, R. M.; Patrocínio, A. O. T.; Machado, A. E. H. *RSC Advances*, **2015**, *5*, 103753. [Crossref]

[25] Cheng, H.; Ma, J.; Zhao, Z.; Qi, L. *Chem. Mater.* **1995**, *7*, 663. [Crossref]

[26] Li, A.; Jin, Y.; Muggli, D.; Pierce, D. T.; Aranwela, H.; Marasinghe, G. K.; Knutson, T.; Brockman, G.; Zhao, J. X. *Nanoscale* **2013**, *5*, 5854. [Crossref]

[27] Liu, C. S.; Li, F. *Opt. Commun.* **2012**, *285*, 2868. [Crossref]

[28] Machado, A. E. H.; França, M. D.; Velani, V.; Magnino, G. A.; Velani, H. M. M.; Freitas, Freitas, F. S.; Muller Jr, P. S.; Sattler, C.; Schmucker, M. *Int. J. Photoenergy* **2008**, 482373. [Crossref]

[29] Tan, L. L; Ong, W. J; Chai, S. P; Mohamed, A. R. *Chem. Commun*, **2014**, *50*, 6923. [Crossref]

[30] Nekrashevich, S.; Gritsenko, V. *Phys. Solid State* **2014**, *56*, 207. [Crossref]

[31] Chia-Ming, W.; Peng, R.; Dimitrijevic, N. M.; Rajh, T.; Koodali, R. T. *Int. J. Hydrogen Energy* **2014**, *39*, 127. [Crossref]

[32] Panwar, K.; Jassal, M.; Agrawal, A. K. *RSC Advances* **2016**, *6*, 92754. [Crossref]

[33] Kermadi, S.; Agoudjil, N.; Sali, S.; Zougar, L.; Boumaour, M.; Broch, L.; En Naciri, A.; Placido, F. *Spectrochim. Acta, Part A*. **2015**, *145*, 145. [Crossref]

[34] Mohamed, M. M.; Osman, G.; Khairou, K. S. *J. Environ. Chem. Eng.* **2015**, *3*, 1847. [Crossref]

[35] Poo-arporn, Y.; Kityakarn, S.; Niltharach, A.; Smith, M. F.; Seraphin, S.; Worner, M.; Worayingyong, A. *Mater. Sci. Semicond. Process.* **2019**, *93*, 21. [Crossref]

[36] Pakdel, E.; Daoud, W. A.; Seyedin, S.; Wang, J.; Razal, J. M. Sun, L.; Wang, X. *Colloids Surf., A* **2018**, *522*, 130. [Crossref]

[37] IUPAC. *Pure Appl. Chem.* **1985**, *57*, 603. [Crossref]

[38] Zhang, X.; Yang, H.; Zhang, F.; Cham, K. Y. *Mater. Lett.* **2007**, *61*, 2231. [Crossref]

[39] Bernardes, A. A.; Bulhosa, M. C.; Gonçalves, F. F.; Montes D'Oca, M. G.; Wolke, S. I. *Quim. Nova* **2011**, *34*, 1343. [Crossref]

[40] Machado, A. E. H.; Miranda, J. A.; Freitas, R. F.; Duarte, E. T. F. M.; Ferreira, I. F.; Albuquerque, Y. D. T.; Ruggiero, R.; Sattler, C.; Oliveira, I. *J J. Photochem. Photobiol., A* **2003**, *155*, 231. [Crossref]

[41] França, M. D.; Santos, L. M.; Silva, T. A.; Borges, K. A.; Silva, V. M.; Patrocinio, A. O. T.; Trovó, A. G.; Machado, A. E. H. *J. Braz. Chem. Soc.* **2016**, *27*,1094. [Crossref]

[42] Yang, X.; Fu, H.; Yu, A.; Jiang, X. J. *Colloid Interface Sci.* **2012**, *387*, 74. [Crossref]

[43] Oliveira, D. F. M.; Batista, P. S.; Muller Jr, P. S.; Velani, V. França, M. D.; Souza, D. R.; Machado, A. E. H. *Dyes Pigm.* **2011**, *92*, 563. [Crossref]

[44] Xie, M. Y.; Su, K. Y.; Peng, X, Y.; Wu, R. J.; Chavali, M.; Chang, W. C. *J. Taiwan Inst. Chem. Eng.* **2017**, *70*, 161. [Crossref]

[45] Zhu, Z.; Chen, J. Y.; Su, K. Y.; Wu, R, J. *J. Taiwan Inst. Chem. Eng.* **2016**, *60*, 222. [Crossref]

[46] Mutuma, B. K.; Shao, G. N.; Kim, W. D.; Kim, H. T. *J. Colloid Interface Sci.*, **2015**, *442*, 1. [Crossref]

[47] Stöber, W., Fink, A., Bohn, E. *J. Colloid Interface Sci.* **1968**, *26*, 62. [Crossref]

90

Orbital: Electron. J. Chem. 11 (2): 83-90, 2019